sciendo
ISSN 1335-8871
MEASUREMENT SCIENCE REVIEW
Journal homepage: https://content.sciendo.com

Investigation of Flux Transfer along Ferrite Core of Probe Coil for Eddy Current Nondestructive Evaluation

Siquan Zhang

Department of Electrical and Automation, Shanghai Maritime University, 1550 Haigang Avenue, Pudong District, 201306, Shanghai, China, sqzhang@shmtu.edu.cn

Abstract: A probe coil with a T-core above a layered conductor with surface hole is investigated for magnetic flux transfer along the ferrite core and enhancement of eddy currents in conductor. The cylindrical coordinate system is adopted and an artificial boundary is added to the solution domain with radius b, and the general formula for calculating the impedance of the T-core coil is derived using the truncated region eigenfunction expansion (TREE) method. For four special cases with different probe configurations, coil impedance changes due to the layered conductor and defect are calculated with Mathematica software over a frequency change ranging from 100 Hz to 20 kHz. The analytical results are in good agreement with those obtained by the finite element method and experimental measurements. The results show that under the same lift-off height and excitation frequency, the impedance change caused by the conductor or defect in the coil of long core column is greater than that of the short core column coil. It indicates that the probe coil with a long core column can transfer magnetic flux to the conductor, thereby enhancing eddy currents in the conductor.

Keywords: Coil impedance, eddy current testing, magnetic flux transfer, layered conductor, T-cored core.

1. INTRODUCTION

Eddy current non-destructive testing (ECT) is an important technique for quantitatively detecting defects such as cracks and corrosion in multilayer conductive structures. Higher magnetic flux density can be achieved by using ferrite core probes to gather magnetic flux and shield noise [1], [2]. I-, E- and C-cored probes are widely used in non-destructive testing of conductive materials and have been proved to have significant advantages over air-cored coils in defect detection [3]-[5].

Under the condition of the same number of turns and coil size, the proposed T-cored coil, shown in Fig. 1, has been proved to have higher magnetic flux concentration effect than the I-cored coil. Compared to the E-cored coil, the T-cored coil is smaller and easier to apply in reality, and its defect detection sensitivity is similar to that of the E-cored coil [6], [7].

Desjardins investigated the detection of deep defects in fastened conductive structures using the ECT method. To avoid removing the fastener, fasteners made of ferromagnetic material have been used as conduits to transfer the magnetic flux into the multilayer conductor [8]. The relationship between the excitation of ferrite fastener and the eddy currents generated in the surrounding aluminum structure was also investigated. The results indicate that the fastener can transmit the magnetic flux into the aluminum structure near the bolt hole, resulting in a strong eddy current response, which is helpful for the detection of deep cracks [9]. Horan et al. analyzed the pulsed eddy current signal generated by a probe that utilized ferromagnetic bolts as magnetic channels to detect simulated cracks inside the spar beneath the wing skin [10]. Whalen came to the conclusion that a ferrite core with a larger diameter than the head of a ferromagnetic fastener would result in deeper penetration of eddy currents. This is due to the larger diameter of the core than the fastener head, allowing increased magnetic flux to be transferred to the fastener. As more magnetic flux penetrates the fastener, more eddy currents are induced in the surrounding conductive structure [11].

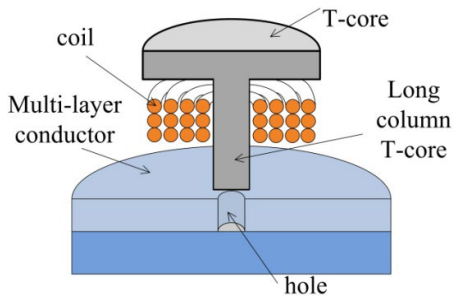

Fig. 1. A T-core coil probe over layered conductor with a hole in the upper layer.

DOI: 10.2478/msr-2023-0002

In addition to the above-mentioned ferromagnetic bolts of the multilayer conducting structure, the core of ferrite cored coil, especially the T-shaped core is also beneficial to transfer the magnetic flux to the conductor, which has the potential to improve the defect detection sensitivity of the coil. However, the influence of magnetic flux transfer along the ferrite core on coil impedance changes has not been investigated using an analytical model. As shown in Fig. 1, a T-core coil is placed above a two-layer conductor with a hole. The influence of magnetic flux transmission along the T-core on the probe sensitivity is investigated, which is helpful to expand the application of the T-core probe in eddy current testing [6], [7].

The analytical model of a T-core probe located on layered conductive materials is derived using the truncated region eigenfunction expansion (TREE) method [12], [13]. The azimuthal component A_φ of the magnetic vector potential is represented by a series of orthogonal eigenfunctions. On the truncation boundary $r = b$, a Dirichlet boundary condition for A_φ is imposed. The most important advantage of the TREE method is that in the truncated finite region, the solution can be expressed in series form rather than integral form, and by carefully choosing discrete eigenvalues and corresponding eigenfunctions, the field continuity of different boundaries and interfaces can be satisfied simultaneously. The numerical calculation efficiency is high and the error control is simple [14], [15].

First, the single-turn coil is analyzed and the expression of the magnetic vector potential in each region is deduced. Then the closed expression for the impedance of the multi-turn coil around the T-core is obtained using the superposition method. As shown in Fig. 1, the length of the T-core column is greater than the thickness of the coil, and the cylindrical coil can move up and down along the T-core column. For four cases with different coil and probe configurations, the coil impedance changes due to the layered conductor or hole are calculated using the derived general expression, and the results are verified by the finite element method or experiments.

2. ANALYSIS

The first configuration to be analyzed is shown in Fig. 2(a), in which a T-core column with relative magnetic permeability μ_f is surrounded by a filamentary coil excited with a sinusoidal current $Ie^{j\omega t}$. The T-core probe is located above a two-layer conductor with conductivities σ_6 and σ_7, and a cylindrical hole of radius c is in the upper layer conductor. The T-core, coil, hole and layered conductor are axisymmetric. A cylindrical coordinate system is established, and the plane $z = 0$ coincides with the upper surface of the conductor. The whole space is truncated by a cylinder of radius $r = b$ and seven regions are formed according to the problem. Using Bessel functions J_n and Y_n, the problem is solved as a boundary value electromagnetic field problem [7].

Since regions 2, 3 and 4 in Fig. 2(a) contain two sub-regions, the magnetic core and the air, these two sub-regions have radial dependencies in the magnetic vector potentials. The equations are obtained using the continuity of B_r and H_z on the interfaces $r = a_2$ and $r = a_1$, and the condition $A_\varphi(b, z) = 0$ must be satisfied at the truncation boundary $r = b$, the following equations can be obtained for solving the eigenvalues m_i and p_i [1].

$$L_1(m_i b) = B_{1F} J_1(m_i b) + C_{1F} Y_1(m_i b) = 0\,, \tag{1}$$

$$R_1(p_i b) = B_{2F} J_1(p_i b) + C_{2F} Y_1(p_i b) = 0\,, \tag{2}$$

where

$$L_1(m_i r) = B_{1F} J_1(m_i r) + C_{1F} Y_1(m_i r)\,, \tag{3}$$

$$R_1(p_i r) = B_{2F} J_1(p_i r) + C_{2F} Y_1(p_i r)\,. \tag{4}$$

The eigenvalues m_i and p_i are the positive real roots of (1) and (2), respectively [1].

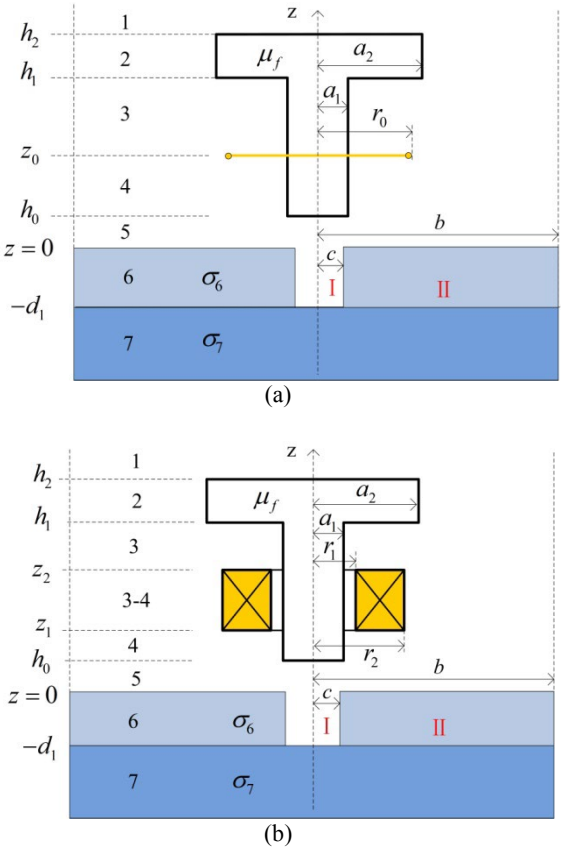

Fig. 2. An axisymmetric (a) filamentary and (b) multi-turn coil T-core probe located over a layered conductor with a hole in the upper layer.

Region 6 consists of two sub-regions of air ($0 \le r \le c$) and conductor ($c \le r \le b$). The magnetic vector potentials of these sub-regions can be expressed. Using the radial interface condition on $r = c$, the equation is obtained and used to determine the eigenvalues u_i and the correlation values v_i.

$$u_i F_1(v_i c) J_0(u_i c) = \frac{1}{\mu_6} v_i F_0(v_i c) J_1(u_i c)\,, \tag{5}$$

where

$$F_n(v_i r) = J_n(v_i r) Y_1(v_i b) - J_1(v_i b) Y_n(v_i r)\,, \tag{6}$$

J_i and Y_i are first kind Bessel functions of i-th order.

The relationship between u_i and v_i satisfies

$$u_i = \sqrt{v_i^2 + j\omega\sigma_6\mu_0\mu_6}\ . \tag{7}$$

Using the method of separation of variables, the expressions of magnetic vector potential in all regions of the problem in Fig. 2(a) can be written in matrix notation as follows:

$$\mathbf{A}_1(r,z) = J_1(\mathbf{q}^{\mathrm{T}}r)\mathbf{q}^{-1}e^{-\mathbf{q}z}\mathbf{C}_1, \tag{8}$$

$$\mathbf{A}_2(r,z) = \frac{J_1(\mathbf{m}^{\mathrm{T}}r)}{L_1(\mathbf{m}^{\mathrm{T}}r)}\mathbf{m}^{-1}(e^{-\mathbf{m}z}\mathbf{C}_2 - e^{\mathbf{m}z}\mathbf{B}_2) \quad \begin{matrix} 0 \le r \le a_2 \\ a_2 \le r \le b \end{matrix}, \tag{9}$$

$$\mathbf{A}_3(r,z) = \frac{J_1(\mathbf{p}^{\mathrm{T}}r)}{R_1(\mathbf{p}^{\mathrm{T}}r)}\mathbf{p}^{-1}(e^{-\mathbf{p}z}\mathbf{C}_3 - e^{\mathbf{p}z}\mathbf{B}_3) \quad \begin{matrix} 0 \le r \le a_1 \\ a_1 \le r \le b \end{matrix}, \tag{10}$$

$$\mathbf{A}_4(r,z) = \frac{J_1(\mathbf{p}^{\mathrm{T}}r)}{R_1(\mathbf{p}^{\mathrm{T}}r)}\mathbf{p}^{-1}(e^{-\mathbf{p}z}\mathbf{C}_4 - e^{\mathbf{p}z}\mathbf{B}_4) \quad \begin{matrix} 0 \le r \le a_1 \\ a_1 \le r \le b \end{matrix}, \tag{11}$$

$$\mathbf{A}_5(r,z) = J_1(\mathbf{q}^{\mathrm{T}}r)\mathbf{q}^{-1}(e^{-\mathbf{q}z}\mathbf{C}_5 - e^{\mathbf{q}z}\mathbf{B}_5), \tag{12}$$

$$\mathbf{A}_6 = \frac{F_1(\mathbf{v}c)J_1(\mathbf{u}^{\mathrm{T}}r)}{F_1(\mathbf{v}^{\mathrm{T}}r)J_1(\mathbf{u}c)}\mathbf{u}^{-1}(e^{-\mathbf{u}z}\mathbf{C}_6 - e^{\mathbf{u}z}\mathbf{B}_6) \quad \begin{matrix} 0 \le r \le c \\ c \le r \le b \end{matrix}, \tag{13}$$

$$\mathbf{A}_7(r,z) = -J_1(\mathbf{q}^{\mathrm{T}}r)\mathbf{k}^{-1}e^{\mathbf{k}z}\mathbf{B}_7, \tag{14}$$

where

$$\mathbf{k} = \sqrt{\mathbf{q}^{\,2} + j\omega\mu_7\mu_0\sigma_7}\ . \tag{15}$$

$J_1(\mathbf{q}^{\mathrm{T}}r)$, $J_1(\mathbf{m}^{\mathrm{T}}r)$, $L_1(\mathbf{m}^{\mathrm{T}}r)$, $J_1(\mathbf{p}^{\mathrm{T}}r)$, $R_1(\mathbf{p}^{\mathrm{T}}r)$, $J_1(\mathbf{u}^{\mathrm{T}}r)$, are row vectors, $\mathbf{q}^{-1}$, $\mathbf{m}^{-1}$, $\mathbf{p}^{-1}$, $\mathbf{u}^{-1}$, $\mathbf{k}^{-1}$, $e^{\pm\mathbf{q}z}$, $e^{\pm\mathbf{m}z}$, $e^{\pm\mathbf{p}z}$, $e^{\pm\mathbf{u}z}$, $e^{\mathbf{k}z}$ are diagonal matrices, and $\mathbf{C}_i$, $\mathbf{B}_i$ are unknown column vector coefficients.

The interface conditions (continuity of B_z and H_r) between the seven regions are used to solve the unknown coefficients in (8)-(14), then the magnetic vector potentials in all regions in Fig. 2(a) can be calculated.

The eigenvalues q_i of regions 1, 5 and 7 are the positive real roots of the following equation:

$$J_1(q_i b) = 0 \qquad i = 0,1,2...N_s\ , \tag{16}$$

where N_s is the highest term in the expansion.

The eigenvalues m_i and p_i are real positive numbers, and can be obtained by solving equations (1) and (2) using numerical methods, such as FindRoot( ) in Mathematica or fzero( ) in Matlab.

The solution of the eigenvalues u_i can be obtained by solving (5) using numerical methods, such as the Newton-Raphson technique [12] or the Cauchy argument principle [16]. The former usually requires to indicate initial points for searching complex roots. For the problem of a hole in the conductor, air and conductor without a hole are used as two sets of initial points, respectively. The advantage of the Newton-Raphson technique is that it is fast in computation, but some eigenvalues can be omitted, or the same root can be obtained for different starting points [12]. The Cauchy argument principle method first checks the number of roots inside the contour constituting the solution domain, and then divides the contour into smaller parts until each part has no more than three roots. Although the accuracy of the Cauchy argument principle method is high, the calculation time is long and cannot be applied in real-time measurement [16]. Based on the Cauchy argument principle method, some new algorithms with good reliability and efficiency have been proposed [17], [18]. A solution combining the advantages of the above two methods was proposed. All complex eigenvalues can be calculated without consuming too much time [19].

First, the magnetic vector potentials $A_{(l)\text{filamentary}}$, $l = 1, 2,\ldots 7$ of all regions excited by a single-turn coil, as shown in Fig. 2(a), are obtained. Then a superposition is applied to calculate the magnetic vector potentials of all regions excited by a multi-turn coil shown in Fig. 2(b) as follows:

$$A_l^{coil}(r,z) = \int_{r_1}^{r_2}\int_{z_1}^{z_2} A_{(l)\,filamentary}(r,z,r_0,z_0)dr_0dz_0\ . \tag{17}$$

In Fig. 2(b), the magnetic vector potential A_{3-4}^{coil} of the region 3-4 is obtained by replacing z_2 in A_3^{coil} with z and z_1 in A_4^{coil} with z and adding them together. Finally, the superposition principle is applied again to derive the coil impedance of multi-turn as follows:

$$\begin{aligned} Z &= \frac{j\omega 2\pi N}{I(z_2-z_1)(r_2-r_1)}\int_{r_1}^{r_2}\int_{z_1}^{z_2} rA_{3-4}^{coil}(r,z)drdz \\ &= \frac{j\omega\mu\pi N^2}{(r_2-r_1)^2(z_2-z_1)^2}\cdot\mathbf{p}^{-4}\cdot\chi(\mathbf{p}r_1,\mathbf{p}r_2) \\ &\cdot[2(z_2-z_1)\mathbf{p} + e^{\mathbf{p}(z_1-z_2)} - e^{\mathbf{p}(z_2-z_1)} + \mathbf{W}_1\mathbf{W}_2^{-1}\mathbf{W}_3] \\ &\cdot\mathbf{D}^{-1}\cdot\mathbf{p}^{-3}\cdot\chi(\mathbf{p}r_1,\mathbf{p}r_2) \end{aligned}, \tag{18}$$

where I is the current carried in each wire loop.

$$\chi(x_1,x_2) = \int_{x_1}^{x_2} xR_1(x)dx\ , \tag{19}$$

$$\mathbf{W}_1 = (e^{-\mathbf{p}z_1} - e^{-\mathbf{p}z_2})\mathbf{C}_{47} - (e^{\mathbf{p}z_2} - e^{\mathbf{p}z_1})\mathbf{B}_{47}, \tag{20}$$

$$\begin{aligned} \mathbf{W}_2 = {} & (\boldsymbol{\lambda}_1\mathbf{F}^{-1}\mathbf{G} + \boldsymbol{\lambda}_2\mathbf{F}^{-1}\mathbf{G}^*)e^{-\mathbf{p}h_1}\mathbf{C}_{47} \\ & -(\boldsymbol{\lambda}_1\mathbf{F}^{-1}\mathbf{G} - \boldsymbol{\lambda}_2\mathbf{F}^{-1}\mathbf{G}^*)e^{\mathbf{p}h_1}\mathbf{B}_{47} \end{aligned}, \tag{21}$$

$$\begin{aligned} \mathbf{W}_3 = {} & (\boldsymbol{\lambda}_1\mathbf{F}^{-1}\mathbf{G} - \boldsymbol{\lambda}_2\mathbf{F}^{-1}\mathbf{G}^*)(e^{\mathbf{p}(h_1-z_1)} - e^{\mathbf{p}(h_1-z_2)}) \\ & -(\boldsymbol{\lambda}_1\mathbf{F}^{-1}\mathbf{G} + \boldsymbol{\lambda}_2\mathbf{F}^{-1}\mathbf{G}^*)(e^{\mathbf{p}(z_2-h_1)} - e^{\mathbf{p}(z_1-h_1)}) \end{aligned}, \tag{22}$$

$$\begin{matrix} \boldsymbol{\lambda}_1 \\ \boldsymbol{\lambda}_2 \end{matrix} = (\mathbf{T}-\mathbf{U})e^{\mathbf{m}(h_1-h_2)} \pm (\mathbf{T}+\mathbf{U})e^{\mathbf{m}(h_2-h_1)}, \tag{23}$$

$$\begin{matrix} \mathbf{C}_{47} \\ \mathbf{B}_{47} \end{matrix} = \frac{1}{2}e^{\pm\mathbf{p}h_0}[(\mathbf{H}^{-1} \pm \mathbf{N}^{-1})\mathbf{E}e^{-\mathbf{q}h_0}\mathbf{C}_{57} + (\mathbf{N}^{-1} \mp \mathbf{H}^{-1})\mathbf{E}\ e^{\mathbf{q}h_0}\mathbf{B}_{57}] \tag{24}$$

$$\begin{matrix}\mathbf{C}_{57}\\ \mathbf{B}_{57}\end{matrix}=\frac{1}{2}\mathbf{E}^{-1}[(\mathbf{M}\pm\mathbf{K})\mathbf{C}_{67}+(\mathbf{K}\mp\mathbf{M})\mathbf{B}_{67}], \tag{25}$$

$$\begin{matrix}\mathbf{C}_{67}\\ \mathbf{B}_{67}\end{matrix}=\frac{1}{2}e^{\mp\mathbf{u}d_1}(\mathbf{K}^{-1}\mathbf{E}\mp\mathbf{M}^{-1}\mathbf{E}\mathbf{q}\mathbf{k}^{-1})e^{-\mathbf{k}d_1}, \tag{26}$$

where

$$\mathbf{C}_{n7}=\frac{\mathbf{C}_n}{\mathbf{B}_7}, \tag{27}$$

$$\mathbf{B}_{n7}=\frac{\mathbf{B}_n}{\mathbf{B}_7}. \tag{28}$$

The definitions of matrices T, U, F, G, G*, N, H, M, K, D, and E are expressed in the appendix.

3. SPECIAL CASES

In order to investigate the transfer of magnetic flux along the T-core column for detecting the layered conductor and defect, several cases shown in Fig. 3 are examined. Fig. 3(a) shows the coil located at the uppermost position of the T-core column, and Fig. 3(b) shows the coil located at the lowermost position of the T-core column. The positions of the coil and the T-core in Fig. 3(c) are the same as those in Fig. 3(a), except that the part of the T-core column sticking out of the coil is removed. The position of the coil in Fig. 3(d) is the same as in Fig. 3(b), but without the T-core. The coil impedance of the above-mentioned T-core probe over a conductor with a surface hole can be calculated by (18).

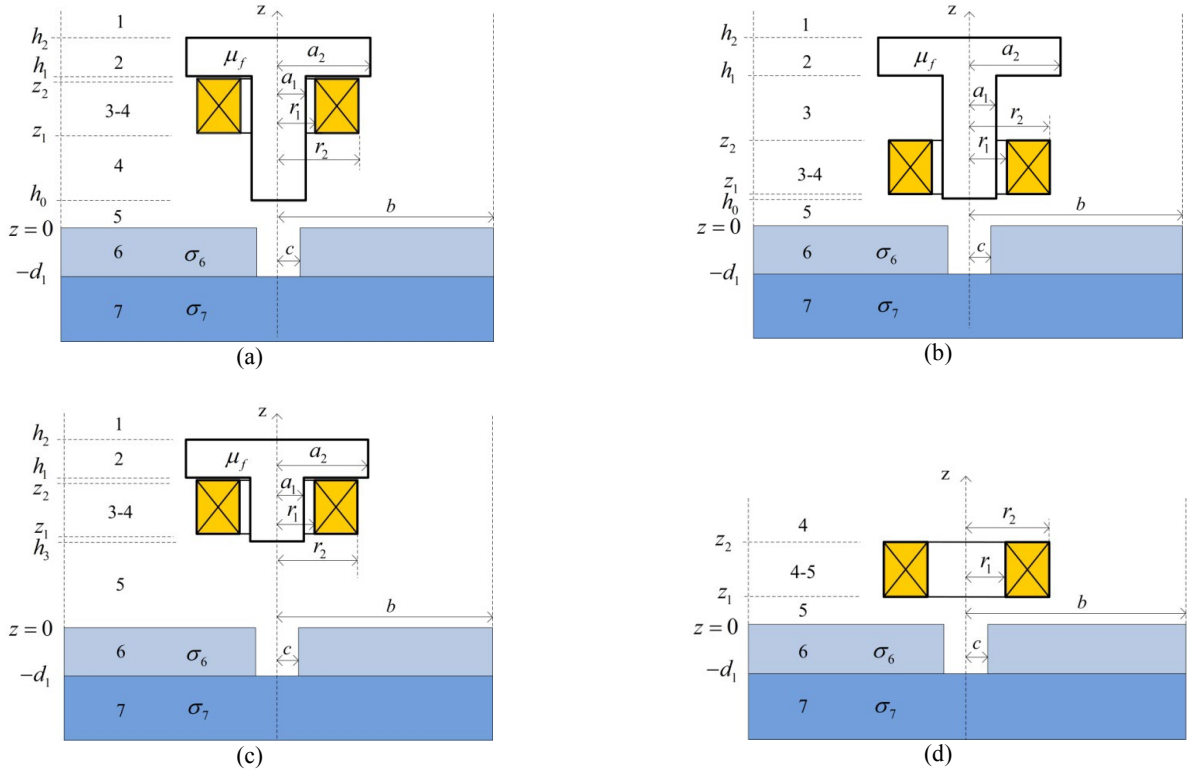

Fig. 3. Several cases of probe configuration (a) The coil at the uppermost position of the T-core column, (b) The coil at the bottom of the T-core column, (c) The coil at the uppermost position of the T-core column with the part extending out the coil removed, (d) Air- cored coil.

For the air-cored coil in Fig. 3(d), the magnetic vector potential in each region is expressed as:

$$\mathbf{A}_4(r,z)=J_1(\mathbf{q}^{\mathrm{T}}r)\mathbf{q}^{-1}e^{-\mathbf{q}z}\mathbf{C}_4, \tag{29}$$

$$\mathbf{A}_5(r,z)=J_1(\mathbf{q}^{\mathrm{T}}r)\mathbf{q}^{-1}(e^{-\mathbf{q}z}\mathbf{C}_5-e^{\mathbf{q}z}\mathbf{B}_5), \tag{30}$$

$$\mathbf{A}_6(r,z)=\frac{J_1(\mathbf{u}^{\mathrm{T}}r)F_1(\mathbf{v}c)}{F_1(\mathbf{v}^{\mathrm{T}}r)J_1(\mathbf{u}c)}\mathbf{u}^{-1}(e^{-\mathbf{u}z}\mathbf{C}_6-e^{\mathbf{u}z}\mathbf{B}_6)\quad\begin{matrix}0\le r\le c\\ c\le r\le b\end{matrix}, \tag{31}$$

$$\mathbf{A}_7(r,z)=-J_1(\mathbf{q}^{\mathrm{T}}r)\mathbf{s}_7^{-1}e^{\mathbf{s}_7 z}\mathbf{B}_7, \tag{32}$$

where

$$\mathbf{u}=\sqrt{\mathbf{v}^2+j\omega\mu_0\mu_6\sigma_6}, \tag{33}$$

$$\mathbf{s}_7=\sqrt{\mathbf{q}^2+j\omega\mu_0\mu_7\sigma_7}. \tag{34}$$

The expression for impedance of the air-cored coil over the layered conductor with surface layer hole can be derived as follows:

$$\begin{aligned}Z=&\frac{j\omega\mu 2\pi N^2}{(r_2-r_1)^2(z_2-z_1)^2}\chi(\mathbf{q}r_1,\mathbf{q}r_2)\mathbf{q}^{-4}\\ &\cdot\{\frac{1}{2}[(z_2-z_1)\mathbf{q}+e^{\mathbf{q}(z_1-z_2)}-1]+\mathbf{W}_1\mathbf{W}_2^{-1}\},\\ &\cdot\mathbf{E}^{-1}\mathbf{q}^{-3}\chi(\mathbf{q}r_1,\mathbf{q}r_2)\end{aligned} \tag{35}$$

where

$$\chi(\mathbf{q}r_1,\mathbf{q}r_2)=\int_{\mathbf{q}r_1}^{\mathbf{q}r_2}(\mathbf{q}r)J_1(\mathbf{q}r)d(\mathbf{q}r)\,, \tag{36}$$

$$\begin{aligned}\mathbf{W_1}=&[(z_2-z_1)\mathbf{q}-1+e^{\mathbf{q}(z_1-z_2)}]\mathbf{B_{57}}\\&+[2e^{-\mathbf{q}(z_1+z_2)}-e^{-2\mathbf{q}z_1}-e^{-2\mathbf{q}z_2}]\mathbf{C_{57}}\end{aligned}, \tag{37}$$

$$\mathbf{W_2}=(\mathbf{E}^{-1}\mathbf{N}-\mathbf{q}\mathbf{E}^{-1}\mathbf{V}\mathbf{u}^{-1})\mathbf{C_{67}}+(\mathbf{E}^{-1}\mathbf{N}+\mathbf{q}\mathbf{E}^{-1}\mathbf{V}\mathbf{u}^{-1})\mathbf{B_{67}}\,, \tag{38}$$

$$\begin{matrix}\mathbf{C_{57}}\\\mathbf{B_{57}}\end{matrix}=\frac{1}{2}[(\mathbf{E}^{-1}\mathbf{N}\pm\mathbf{q}\mathbf{E}^{-1}\mathbf{V}\mathbf{u}^{-1})\mathbf{C_{67}}+(\mathbf{E}^{-1}\mathbf{N}\mp\mathbf{q}\mathbf{E}^{-1}\mathbf{V}\mathbf{u}^{-1})\mathbf{B_{67}}], \tag{39}$$

$$\begin{matrix}\mathbf{C_{67}}\\\mathbf{B_{67}}\end{matrix}=\frac{1}{2}e^{\mp\mathbf{u}d_1}(\mathbf{N}^{-1}\mathbf{E}\mp\mathbf{u}\mathbf{V}^{-1}\mathbf{E}\mathbf{s}_7^{-1})e^{-\mathbf{s}_7d_1}. \tag{40}$$

In order to investigate the impedance change of the T-core coil due to a hole in the conductor, it is necessary to calculate the coil impedance of the T-core coil above the layered conductor of the same material and the same thickness without a hole. If the hole in the conductor in Fig. 2 disappears, the magnetic vector potentials of all regions excited by the single-turn coil can be obtained, and the expression for impedance of the T-cored coil over layered conductor without a hole can be derived as follows [6]:

$$\begin{aligned}Z=&\frac{j\omega\mu\pi N^2}{(r_2-r_1)^2(z_2-z_1)^2}\cdot\mathbf{p}^{-4}\chi(\mathbf{p}r_1,\mathbf{p}r_2)\\&\cdot[2(z_2-z_1)\mathbf{p}+e^{\mathbf{p}(z_1-z_2)}-e^{\mathbf{p}(z_2-z_1)}+\mathbf{W}_1\mathbf{W}_2^{-1}\mathbf{W}_3]\\&\cdot\mathbf{D}^{-1}\mathbf{p}^{-3}\chi(\mathbf{p}r_1,\mathbf{p}r_2)\end{aligned}, \tag{41}$$

where

$$\mathbf{W}_1=(e^{-\mathbf{p}z_1}-e^{-\mathbf{p}z_2})\mathbf{C}_{47}-(e^{\mathbf{p}z_2}-e^{\mathbf{p}z_1})\mathbf{B}_{47}\,, \tag{42}$$

$$\begin{aligned}\mathbf{W_2}=&(\boldsymbol{\lambda}_1\mathbf{F}^{-1}\mathbf{G}+\boldsymbol{\lambda}_2\mathbf{F}^{-1}\mathbf{G}^*)e^{-\mathbf{p}h_1}\mathbf{C}_{47}\\&-(\boldsymbol{\lambda}_1\mathbf{F}^{-1}\mathbf{G}-\boldsymbol{\lambda}_2\mathbf{F}^{-1}\mathbf{G}^*)e^{\mathbf{p}h_1}\mathbf{B}_{47}\end{aligned}, \tag{43}$$

$$\begin{aligned}\mathbf{W}_3=&(\boldsymbol{\lambda}_1\mathbf{F}^{-1}\mathbf{G}-\boldsymbol{\lambda}_2\mathbf{F}^{-1}\mathbf{G}^*)(e^{\mathbf{p}(h_1-z_1)}-e^{\mathbf{p}(h_1-z_2)})\\&-(\boldsymbol{\lambda}_1\mathbf{F}_{ji}^{-1}\mathbf{G}_{ji}+\boldsymbol{\lambda}_2\mathbf{F}_{ji}^{-1}\mathbf{G}_{ji}^*)(e^{\mathbf{p}(z_2-h_1)}-e^{\mathbf{p}(z_1-h_1)})\end{aligned}, \tag{44}$$

4. Experimental verification

The coil, short column and long column T-cores used in experiments are shown in Fig. 4. The T-cores with known relative permeability are selected, and the permeability is corrected by the experimental estimation method [1]. The rectangular cross-section cylindrical coil is self-made. The short column T-core can be used in the situation shown in Fig. 3(c). Since the length of the long T-core column is greater than the height of the cylindrical coil, the coil can move up and down along the T-core column to change the lift-off height of the coil, which can be used in the situations shown in Fig. 3(a) and Fig. 3(b).

The experimental setup is shown in Fig. 5. The probes are arranged above the surface of the layered conductor with a hole, as shown in Fig. 3, the coil impedance is measured by the GWInstek LCR-821 digital LCR meter. The layered conductor is then removed and the impedance of the coil is measured again for each case. The change of coil impedance caused by the layered conductor can be obtained by subtracting the coil impedance without conductor from the coil impedance with conductor. Change the excitation frequency of the coil, and measure the change of coil impedance at different frequencies, respectively.

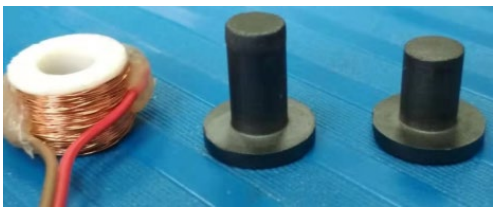

Fig. 4. Coil and T-cores.

Fig. 5. Experimental setup of T-core coil above the layered conductor with a surface hole.

Table 1. Parameters of the coil, core and conductor used in analytical calculations, FEM and experiments.

Coil	Parameter	Value
Inner coil radius	r_1	5.2 mm
Outer coil radius	r_2	7.2 mm
Number of turns	N	416
T-Core	Parameter	Value
Inner core radius	a_1	4 mm
Outer core radius	a_2	8 mm
Liftoff 1	h_0	0.1 mm
Inner core height	h_1	15.4 mm
Outer core height	h_2	17.8 mm
Liftoff 2	h_3	4.3 mm
Relative permeability	μ_f	2000
Conductor	Parameter	Value
Relative permeability	μ_6, μ_7	1
Conductivity	σ_6	36 MS/m
Conductivity	σ_7	36 MS/m
Hole radius	c	4 mm
Thickness	d_1	4 mm
Radius of the domain	b	90 mm

5. Results and discussion

According to (18), Mathematica is used to calculate the coil impedance of the T-core probe located above the layered conductor with a hole. The parameters used in the calculation are shown in Table 1. When calculating the probe configurations as shown in Fig. 3(a) and Fig. 3(c), the parameters are $z_1 = 4.8$ mm and $z_2 = 14.1$ mm. When calculating the cases shown in Fig. 3(b) and Fig. 3(d), the parameters become $z_1 = 0.3$ mm, $z_2 = 9.6$ mm.

The impedance of air-cored coil is calculated with (35). In all calculations, the domain radius is $b = 90$ mm (12.5 times the outer radius of the coil) and the number of summation terms $N_s = 60$.

First, the coil impedance $Z = R + jX$ is calculated when the probe is placed over the conductor with conductivities $\sigma_6 = \sigma_7 = 36$ MS/m, and then the coil impedance $Z_0 = R_0 + jX_0$ is calculated when the conductor is absent ($\sigma_6 = \sigma_7 = 0$). The change of coil resistance due to the layered conductor is denoted as $\Delta R = R - R_0$, and the change of reactance is denoted as $\Delta X = X - X_0$. The analytical calculation results are compared with data of experiments and the finite element method using the ANSYS software package.

Fig. 6 shows the changes of coil impedance on a layered conductor with a hole for four different configurations of probes at different excitation frequencies. Among them, T-core-long-up and T-core-long-low indicate that the coil is located at the uppermost position and bottom of the T-core column, respectively. T-core-short indicates that the coil is located at the uppermost position of the T-core column, but the part extending out of the coil is removed. Air-core is air-cored coil. In all cases, the relative errors of the results of the TREE method, FEM and experiment are less than 2%.

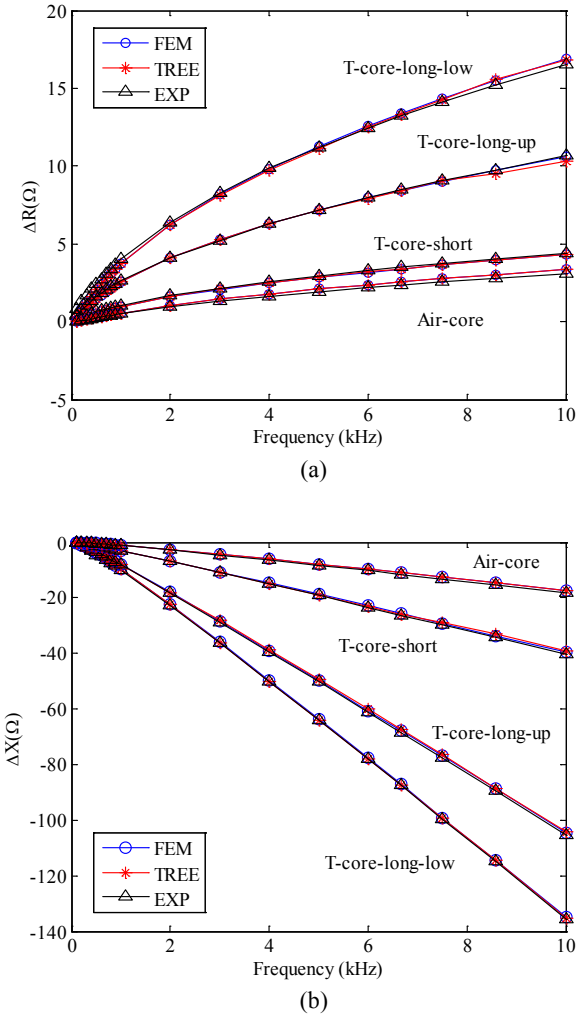

Fig. 6. The changes of coil (a) resistance and (b) reactance as a function of frequency for different cases of probes due to the layered conductor.

In the frequency range from 0 to 10 kHz, when the coil is located at the uppermost position of the core column, the impedance change of the coil with the core extending to the surface of the conductor is larger than that of the coil without the extended core. At a frequency of 10 kHz, the resistance changes of the two coils are 10.6 Ohm and 4.3 Ohm, respectively, the former is almost 2.5 times the latter. The results show that the magnetic flux can be transferred to the conductor along the magnetic core, which enhances the eddy current in the conductor.

The coil impedance change due to the hole in the upper layer conductor is calculated by subtracting the impedance of the coil over the layered conductor without a hole from the impedance of the coil over the layered conductor with a hole. Because the impedance change caused by the hole in the conductor is very small, it is difficult to measure accurately with an LCR meter. Therefore, only the data of FEM are compared with analytical calculated results.

The parameters of coil, T-core and conductor used in the analytical calculation and FEM are shown in Table 2. In order to obtain distinguishable impedance changes in calculation, some of the parameters have been changed.

Table 2. Parameters of the coil, core, and conductor used in analytical calculations and FEM.

Coil	Parameter	Value
Inner coil radius	r_1	4.5 mm
Outer coil radius	r_2	8.5 mm
Number of turns	N	800
T-Core	**Parameter**	**Value**
Inner core radius	a_1	4 mm
Outer core radius	a_2	9 mm
Liftoff 1	h_0	0.5 mm
Inner core height	h_1	14 mm
Outer core height	h_2	16 mm
Liftoff 2	h_3	5.5 mm
Relative permeability	μ_f	500
Conductor	**Parameter**	**Value**
Relative permeability	μ_6 , μ_7	1
Conductivity	σ_6	16 MS/m
Conductivity	σ_7	10 MS/m
Hole radius	c	4 mm
Thickness	d_1	6 mm
Radius of the domain	b	90 mm

When calculating the probe configuration as shown in Fig. 3(a) and Fig. 3(c), the parameters are $z_1 = 5.5$ mm and $z_2 = 13.5$ mm. When calculating the probe situation as shown in Fig. 3(b) and Fig. 3(d), the parameters change to $z_1 = 0.5$ mm and $z_2 = 8.5$ mm. When the situation is as shown in Fig. 3(c), since the part of the core extending out of the coil is removed, the parameter is $h_3 = 5.5$ mm.

According to the parameters in Table 2, the impedance of the coil located on the layered conductor with a hole is calculated by equation (18), denoted as $Z = R + jX$. The impedance of coil located above the conductor without a hole is calculated with (41) and is written as $Z_c = R_c + jX_c$. The changes of coil resistance, reactance and inductance due to the hole in the upper layer conductor are denoted as $\Delta R_c = R - R_c$, $\Delta X_c = X - X_c$ and $\Delta L_c = L - L_c$, respectively. The coil impedance and inductance changes due to the hole of the conductor are also analyzed by the ANSYS software. The results are shown in Fig. 7.

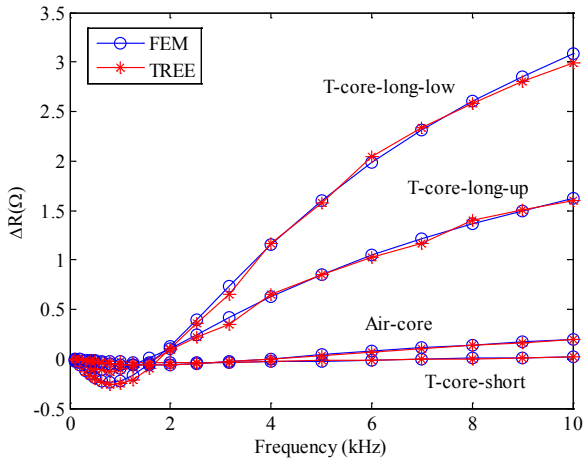

(a)

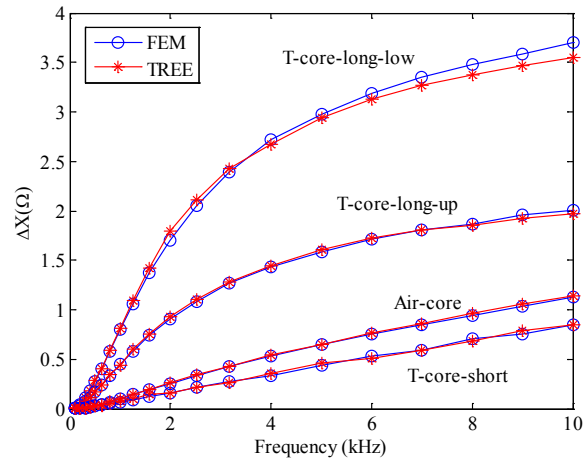

(b)

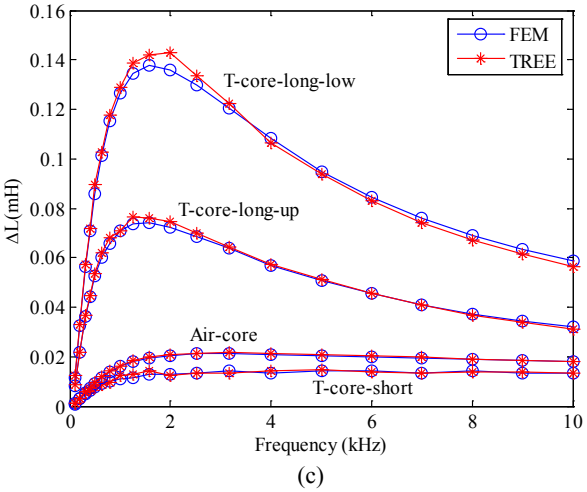

(c)

Fig. 7. The changes of coil (a) resistance, (b) reactance, and (c) inductance as a function of frequency for different cases of probes due to a hole in the upper layer conductor.

For the two probe configurations shown in Fig. 3(a) and Fig. (3c), the excitation frequency is 10 kHz and the lift-off of the coils is the same, the resistance changes of coil due to the hole are 1.62 Ohm and 0.0192 Ohm, respectively, the former is more than 85 times that of the latter. It indicates that the part of the core extending out of the coil can transfer the magnetic flux and enhance the eddy current in the conductor, which is beneficial to the detection of defects.

6. CONCLUSIONS

An analytical model of a T-core probe placed above a conductive half-space layered structure with a hole in the upper layer is proposed. The final expression of the coil impedance is derived using the TREE method. The results show that the ferrite T-core column helps to transfer the magnetic flux to the layered conductor and enhances the eddy current in the layered conductor.

The proposed analytical model can be used for computer simulation of eddy current testing, probe design or directly implemented in eddy current measurement. The effect of magnetic flux transfer along the T-core column can be applied in the eddy current detection of deep defects in a complex layered conductor, such as a fastener hole structure in the layered conductor.

APPENDIX

$$\mathbf{T}=[t_{ij}]=\int_0^{a_2} rJ_0(\mathbf{q}r)J_0(\mathbf{m}^{\mathrm{T}}r)dr+\int_{a_2}^{b} rJ_0(\mathbf{q}r)L_0(\mathbf{m}^{\mathrm{T}}r)dr, \quad \text{(A1)}$$

$$\mathbf{U}=[u_{ij}]=\frac{1}{\mu_f}\int_0^{a_2} rJ_1(\mathbf{q}r)J_1(\mathbf{m}^{\mathrm{T}}r)dr+\int_{a_2}^{b} rJ_1(\mathbf{q}r)L_1(\mathbf{m}^{\mathrm{T}}r)dr, \quad \text{(A2)}$$

$$\mathbf{G}=[g_{ij}]=\int_0^{a_1} rJ_0(\mathbf{m}r)J_0(\mathbf{p}^{\mathrm{T}}r)dr+\int_{a_1}^{a_2} rJ_0(\mathbf{m}r)R_0(\mathbf{p}^{\mathrm{T}}r)dr+\int_{a_2}^{b} rL_0(\mathbf{m}r)R_0(\mathbf{p}^{\mathrm{T}}r)dr, \quad \text{(A3)}$$

$$\mathbf{G}^{*}=[g_{ij}^{*}]=\frac{1}{\mu_f}\int_0^{a_1} rJ_1(\mathbf{m}r)J_1(\mathbf{p}^{\mathrm{T}}r)dr+\int_{a_1}^{a_2} rJ_1(\mathbf{m}r)R_1(\mathbf{p}^{\mathrm{T}}r)dr+\int_{a_2}^{b} rL_1(\mathbf{m}r)R_1(\mathbf{p}^{\mathrm{T}}r)dr, \quad \text{(A4)}$$

$$\mathbf{H}=[h_{ij}]=\int_0^{a_1} rJ_0(\mathbf{q}r)J_0(\mathbf{p}^{\mathrm{T}}r)dr+\int_{a_1}^{b} rJ_0(\mathbf{q}r)R_0(\mathbf{p}^{\mathrm{T}}r)dr, \quad \text{(A5)}$$

$$\mathbf{N}=[n_{ij}]=\frac{1}{\mu_f}\int_0^{a_1} rJ_1(\mathbf{q}r)J_1(\mathbf{p}^{\mathrm{T}}r)dr+\int_{a_1}^{b} rJ_1(\mathbf{q}r)R_1(\mathbf{p}^{\mathrm{T}}r)dr, \quad \text{(A6)}$$

$$\mathbf{M}=[m_{ij}]=F_1(\mathbf{v}^{\mathrm{T}}c)\int_0^{c} rJ_0(\mathbf{q}r)J_0(\mathbf{u}^{\mathrm{T}}r)dr+\mathbf{v}^{\mathrm{T}}\mathbf{u}^{-1}J_1(\mathbf{u}^{\mathrm{T}}c)\int_c^{b} rJ_0(\mathbf{q}r)F_0(\mathbf{v}^{\mathrm{T}}r)dr, \quad \text{(A7)}$$

$$\mathbf{K}=[k_{ij}]=F_1(\mathbf{v}^{\mathrm{T}}c)\int_0^{c} rJ_1(\mathbf{q}r)J_1(\mathbf{u}^{\mathrm{T}}r)dr+J_1(\mathbf{u}^{\mathrm{T}}c)\int_c^{b} rJ_1(\mathbf{q}r)F_1(\mathbf{v}^{\mathrm{T}}r)dr, \quad \text{(A8)}$$

$$\mathbf{E}=[e_{ij}]=\int_0^{b} rJ_0(\mathbf{q}r)J_0(\mathbf{q}^{\mathrm{T}}r)dr=\int_0^{b} rJ_1(\mathbf{q}r)J_1(\mathbf{q}^{\mathrm{T}}r)dr, \quad \text{(A9)}$$

$$\mathbf{F}=[f_{ij}]=\int_0^{a_2} rJ_0(\mathbf{m}r)J_0(\mathbf{m}^{\mathrm{T}}r)dr+\int_{a_2}^{b} rL_0(\mathbf{m}r)L_0(\mathbf{m}^{\mathrm{T}}r)dr, \quad \text{(A10)}$$

$$\mathbf{D}=[d_{ij}]=\frac{1}{\mu_f}\int_0^{a_1} rJ_1(\mathbf{p}r)J_1(\mathbf{p}^{\mathrm{T}}r)dr+\int_{a_1}^{b} rR_1(\mathbf{p}r)R_1(\mathbf{p}^{\mathrm{T}}r)dr. \quad \text{(A11)}$$

REFERENCES

[1] Theodoulidis, T. P. (2003). Model of ferrite-cored probes for eddy current nondestructive evaluation. *Journal of Applied Physics*, 93 (5), 3071-3078. https://doi.org/10.1063/1.1543634

[2] Lu, Y., Bowler, J. R., Theodoulidis, T. P. (2012). An analytical model of a ferrite-cored inductor used as an eddy current probe. *Journal of Applied Physics*, 111 (10), 103907-103910. https://doi.org/10.1063/1.4716189

[3] Tytko, G., Dziczkowski, L. (2018). I-cored coil probe located above a conductive plate with a surface hole. *Measurement Science Review*, 18 (1), 7-12. https://doi.org/10.1515/msr-2018-0002

[4] Zhang, S. (2021). Analytical model of an I-core coil for nondestructive evaluation of a conducting cylinder below an infinite plane conductor. *Measurement Science Review*, 21 (4), 99-105. https://doi.org/10.2478/msr-2021-0014

[5] Tytko, G., Dziczkowski, L. (2019). Calculation of the impedance of an E-cored coil placed above a conductive material with a surface hole. *Measurement Science Review*, 19 (2), 43-47. https://doi.org/10.2478/msr-2019-0007

[6] Zhang, S. (2020). An analytical model of a new T-cored coil used for eddy current nondestructive evaluation. *Applied Computational Electromagnetics Society Journal*, 35 (9), 1099-1104. https://journals.riverpublishers.com/index.php/ACES/article/view/7745

[7] Zhang, S. (2021). Analytical model of a T-core coil above a multi-layer conductor with hidden hole using the TREE method for nondestructive evaluation. *COMPEL - The International Journal for Computation and Mathematics in Electrical and Electronic Engineering*, 40 (6), 1104-1117. https://doi.org/10.1108/COMPEL-03-2021-0099

[8] Desjardins, D., Krause, T. W., Gauthier, N. (2013). Analytical modeling of the transient response of a coil encircling a ferromagnetic conducting rod in pulsed eddy current testing. *NDT&E International*, 60, 127-131. https://doi.org/10.1016/j.ndteint.2013.07.007

[9] Desjardins, D., Vallières, G., Whalen, P. P., Krause, T. W. (2012). Advances in transient (pulsed) eddy current for inspection of multi-layered aluminum structures in the presence of ferrous fasteners. In *Review of Progress in Quantitative Nondestructive Evaluation*: *Volume 31*. AIP Conference Proceedings 1430, 400. https://doi.org/10.1063/1.4716256

[10] Horan, P., Underhill, P. R., Krause, T. W. (2013). Pulsed eddy current detection of cracks in F/A-18 inner wing spar without wing skin removal using Modified Principal Component Analysis. *NDT and E International*, 55, 21-27. https://doi.org/10.1016/j.ndteint.2013.01.004

[11] Whalen, P. P. (2010). *Transient eddy current inspection in the presence of ferrous fasteners in multi-layered aluminum structures*. MASc thesis, Royal Military College of Canada, Kingston, Ontario, Canada. ISBN 9780494718711.

[12] Theodoulidis, T. P., Kriezis, E. E. (2006). *Eddy Current Canonical Problems (With Applications to Nondestructive Evaluation)*. Duluth (Georgia), USA: Tech Science Press, 106-133. ISBN 0-9717880-1-4.

[13] Sakkaki, F., Bayani, H. (2012). Solution to the problem of E-cored coil above a layered half-space using the method of truncated region eigenfunction expansion. *Journal of Applied Physics*, 111 (7), 07E717. https://doi.org/10.1063/1.3675183

[14] Koliskina, V. (2014). Calculation of eigenvalues for eddy current testing problems. *Boundary Field Problems and Computer Simulation*, 53 (1), 9-11. https://doi.org/10.7250/bfpcs.2014.002

[15] Theodoulidis, T. P., Bowler, J. R. (2005). Eddy-current interaction of a long coil with a slot in a conductive plate. *IEEE Transactions on Magnetics*, 41 (4), 1238-1247. https://doi.org/10.1109/TMAG.2005.844838

[16] Davies, B. (1986). Locating the zeros of an analytic function. *Journal of Computational Physics*, 66 (1), 36-49. https://doi.org/10.1016/0021-9991(86)90052-5

[17] Dellnitz, M., Schutze, O., Zheng, Q. (2002). Locating all the zeros of an analytic function in one complex variable. *Journal of Computational and Applied Mathematics*, 138 (2), 325-333. https://doi.org/10.1016/S0377-0427(01)00371-5

[18] Vasic, D., Ambru, D., Bilas, V. (2016). Computation of the eigenvalues for bounded domain eddy current models with coupled regions, *IEEE Transactions on Magnetics*, 52 (6), 1-10. https://doi.org/10.1109/TMAG.2016.2518993

[19] Tytko, G., Dziczkowski, L. (2019). Locating complex eigenvalues for analytical eddy-current models used to detect flaws. *COMPEL - The International Journal for Computation and Mathematics in Electrical and Electronic Engineering*, 38 (6), 1800-1809. https://doi.org/10.1108/COMPEL-03-2019-0130

Received April 22, 2022
Accepted January 05, 2023